US 20140338345A1

(19) **United States**

(12) **Patent Application Publication**

(10) **Pub. No.: US 2014/0338345 A1**

(43) **Pub. Date: Nov. 20, 2014**

Kim et al.

(54) **METHOD AND APPARATUS FOR ENHANCED FLAMEHOLDING IN AUGMENTORS**

(71) Applicant: **The Board of Trustees of the Leland Stanford Junior University**, Palo Alto, CA (US)

(72) Inventors: **Wookyung Kim**, Glastonbury, CT (US); **Mark Godfrey Mungal**, Cupertino, CA (US); **Heinz Guenter Pitsch**, Aachen (DE)

(21) Appl. No.: **13/910,432**

(22) Filed: **Jun. 5, 2013**

Related U.S. Application Data

(63) Continuation-in-part of application No. 12/806,958, filed on Aug. 24, 2010, now abandoned.

(60) Provisional application No. 61/236,456, filed on Aug. 24, 2009.

Publication Classification

(51) **Int. Cl.**
F23R 3/18 (2006.01)

(52) **U.S. Cl.**
CPC ***F23R 3/18*** (2013.01)
USPC **60/749**

(57) **ABSTRACT**

A jet engine flame holder bluffbody is provided that includes a leading edge that is rounded, a mid-body having a rectangular cross-section, and a trailing edge, where the trailing edge includes a rectangular cross-section having digitated cutouts from the rectangular cross-section, where the tailing edge projects upward according to a digitated cross-section, where material digits remain between consecutive pairs of the digitated cutouts.

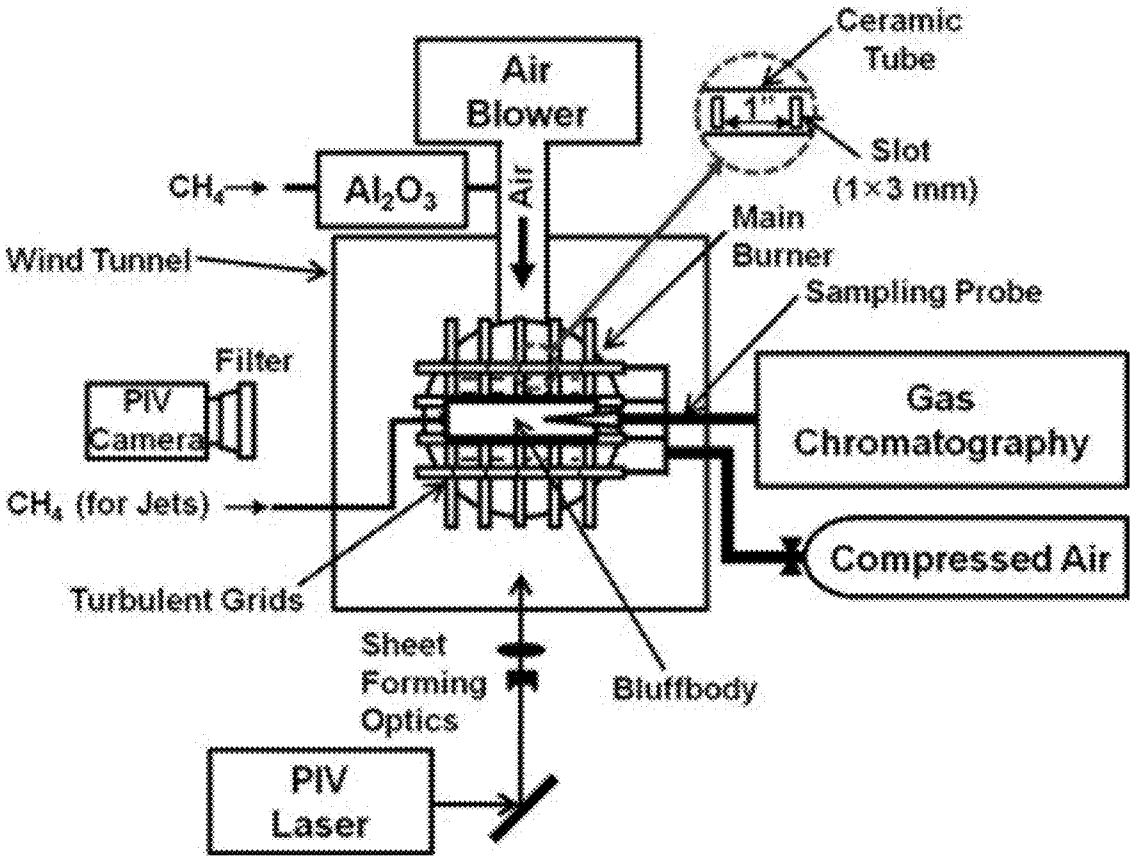

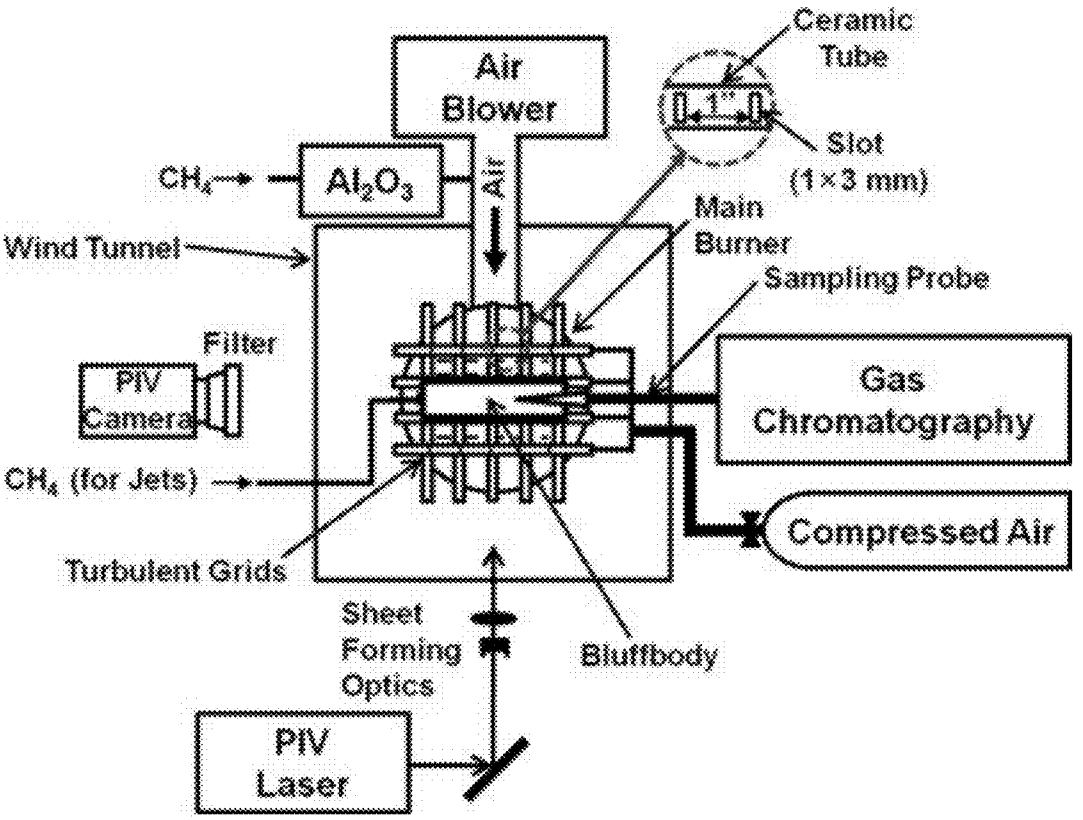
Ceramic Tube
Air Blower
1"
Slot (1×3 mm)
CH_4
Al_2O_3
Air
Main Burner
Wind Tunnel
Sampling Probe
Filter
PIV Camera
Gas Chromatography
CH_4 (for Jets)
Compressed Air
Turbulent Grids
Sheet Forming Optics
Bluffbody
PIV Laser

FIG. 1

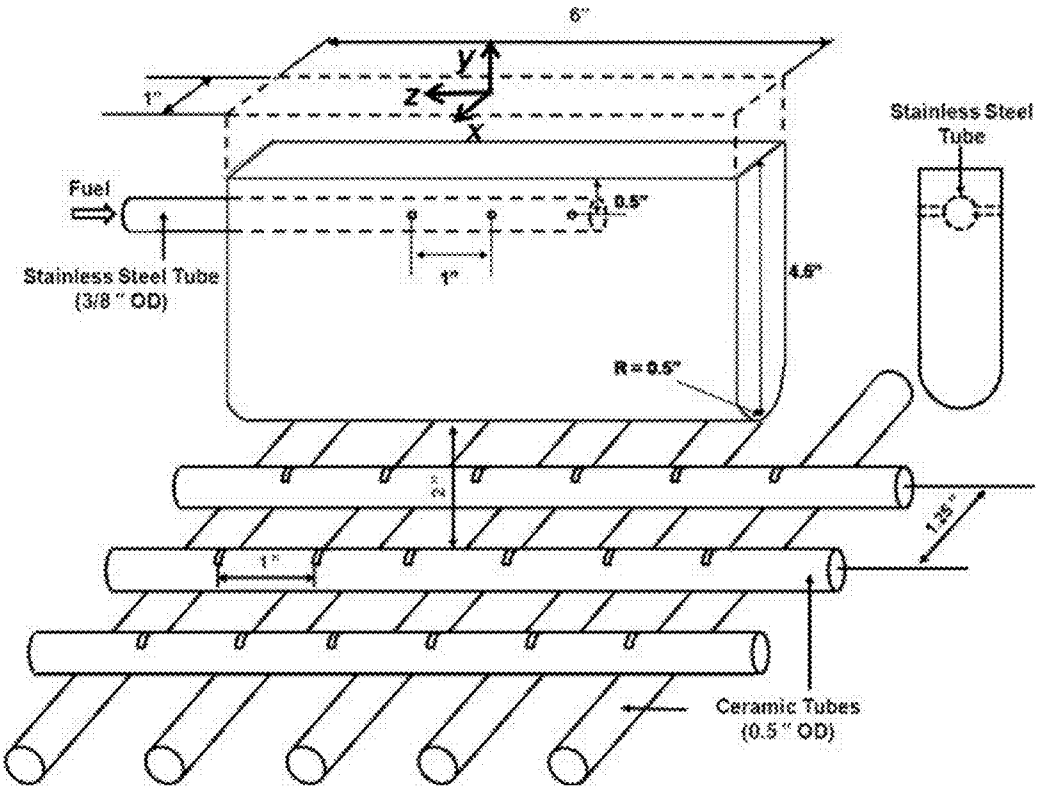
6"
Y
Z
X
1"
Stainless Steel Tube
Fuel
0.5"
Stainless Steel Tube
(3/8 " OD)
1"
4.5"
R = 0.5"
1.25"
1"
Ceramic Tubes
(0.5 " OD)

FIG. 2

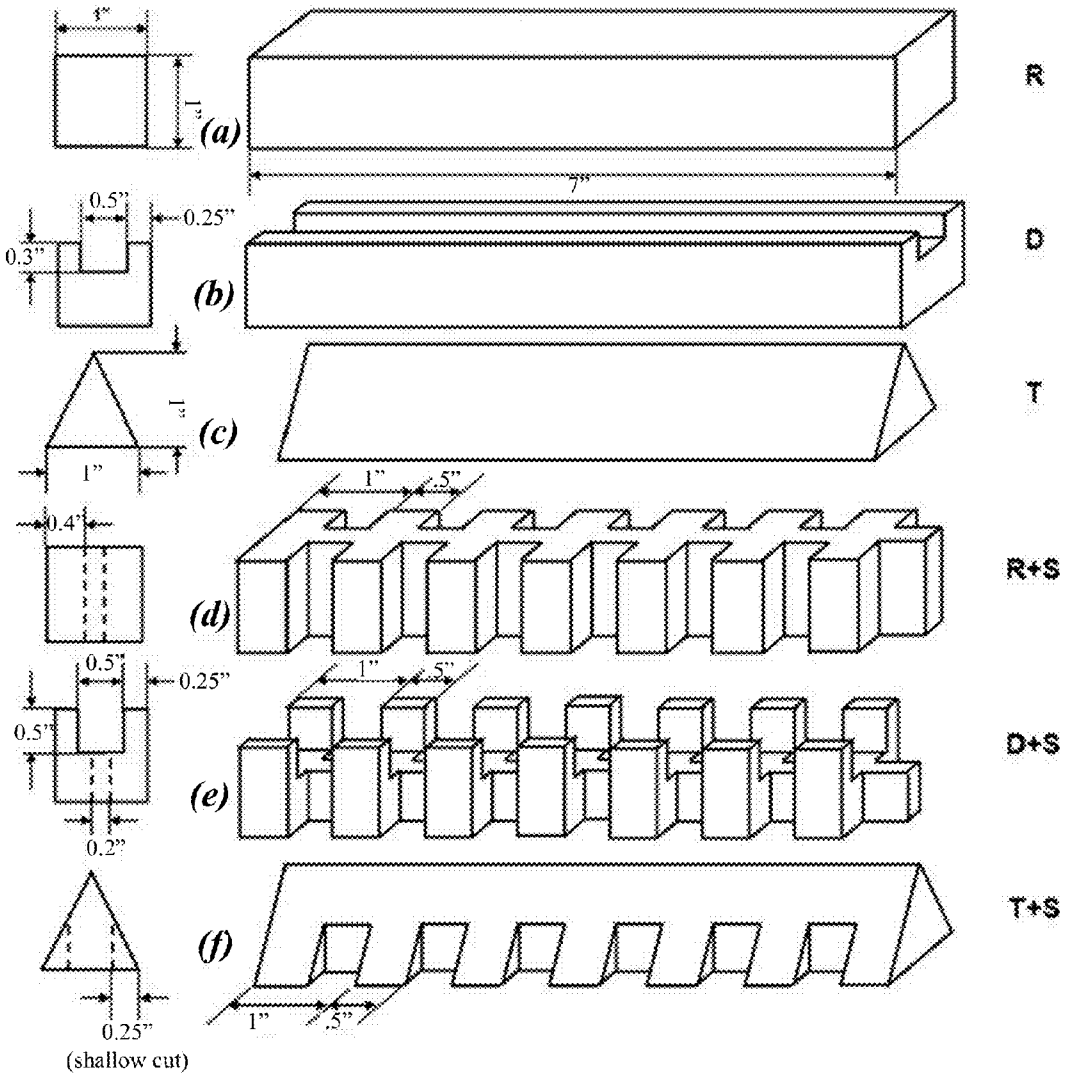
1"
1"
(a)
7"
R
0.5"
0.25"
0.3"
(b)
D
1"
(c)
1"
T
1"
.5"
0.4"
(d)
R+S
0.5"
0.25"
0.5"
1"
.5"
(e)
D+S
0.2"
(f)
T+S
0.25"
(shallow cut)
1"
.5"

FIG. 3

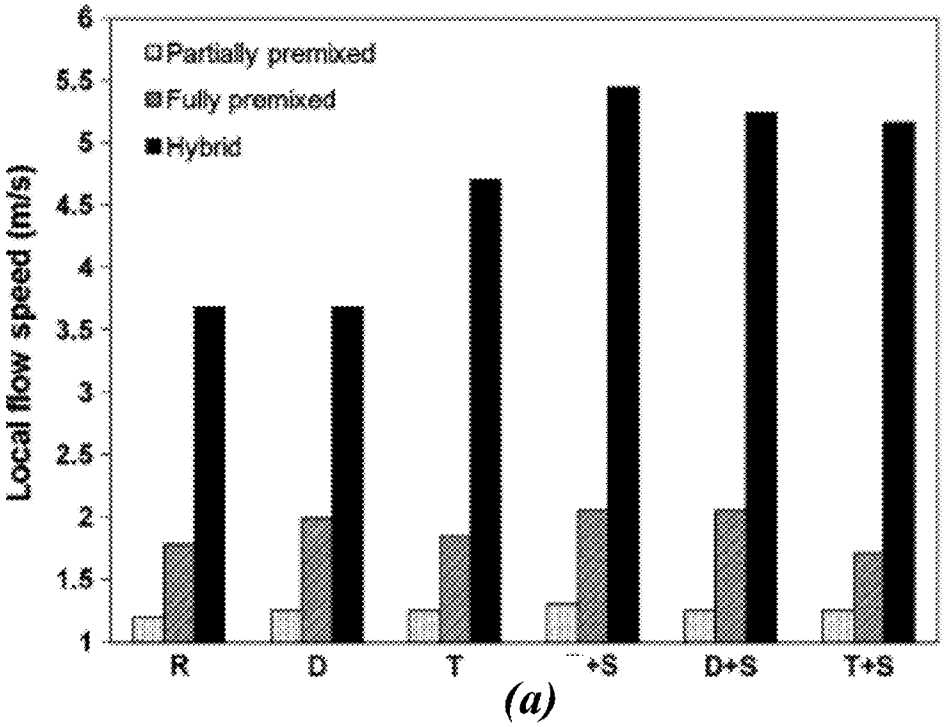
Partially premixed
Fully premixed
Hybrid
Local flow speed (m/s)
6
5.5
5
4.5
4
3.5
3
2.5
2
1.5
1
R
D
T
+S
D+S
T+S

(a)

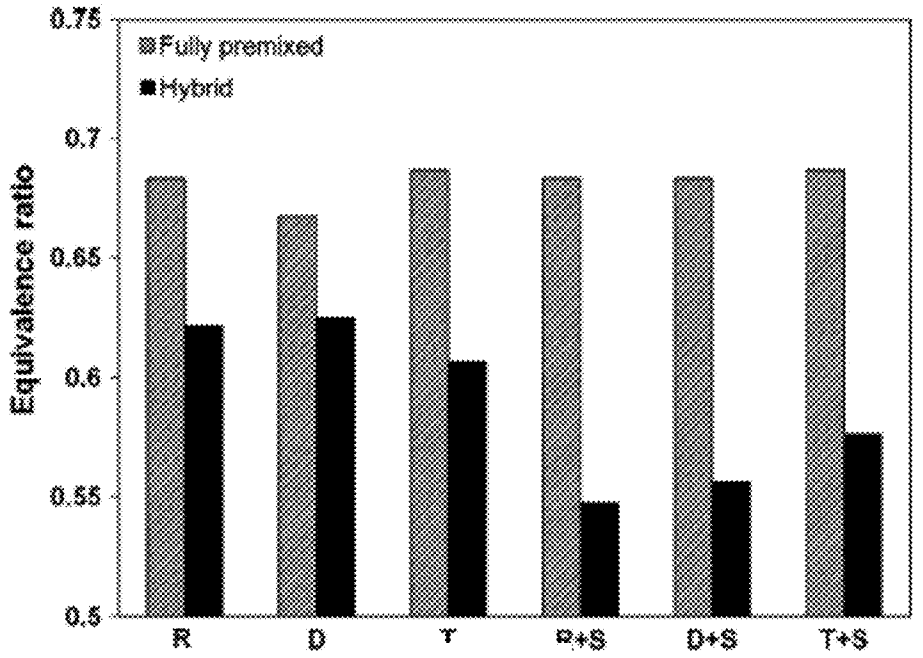
Fully premixed
Hybrid
Equivalence ratio
0.75
0.7
0.65
0.6
0.55
0.5
R
D
T
+S
D+S
T+S

(b)

FIG. 4

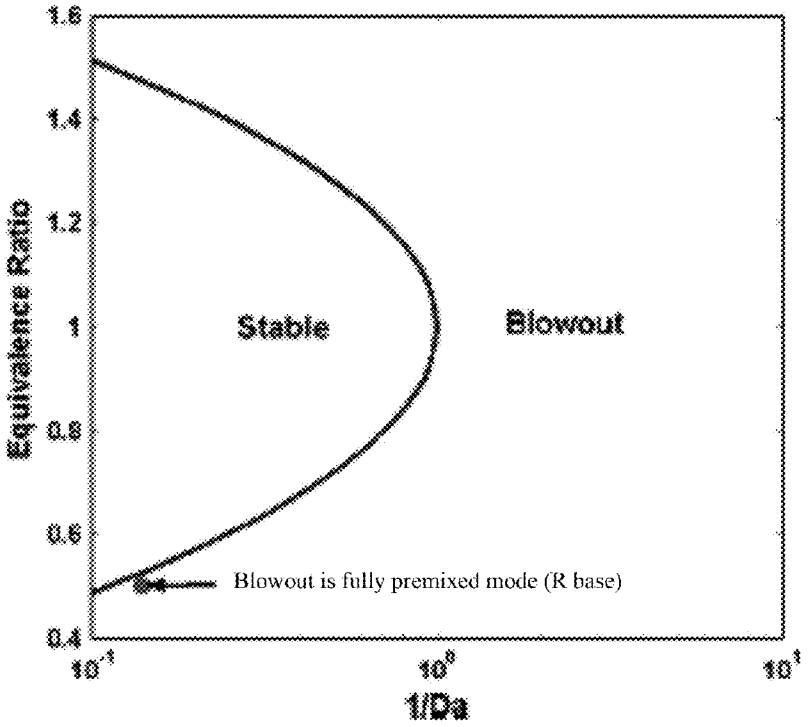
Equivalence Ratio
1.6
1.4
1.2
1
0.8
0.6
0.4
Stable
Blowout
Blowout is fully premixed mode (R base)
10^-1
10^0
10^1
1/Da

FIG. 5

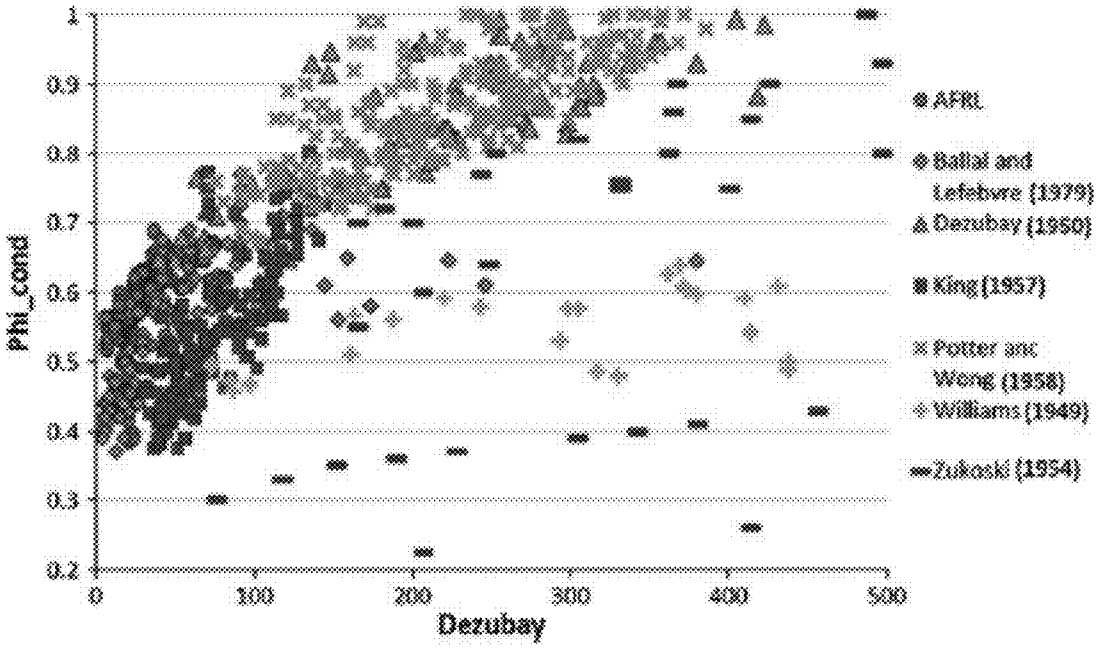
Phi_cond
1
0.9
0.8
0.7
0.6
0.5
0.4
0.3
0.2
0
100
200
300
400
500
Dezubay
AFRL
Ballal and Lefebvre (1979)
Dezubay (1950)
King (1957)
Potter and Wong (1958)
Williams (1949)
Zukoski (1954)

FIG. 6

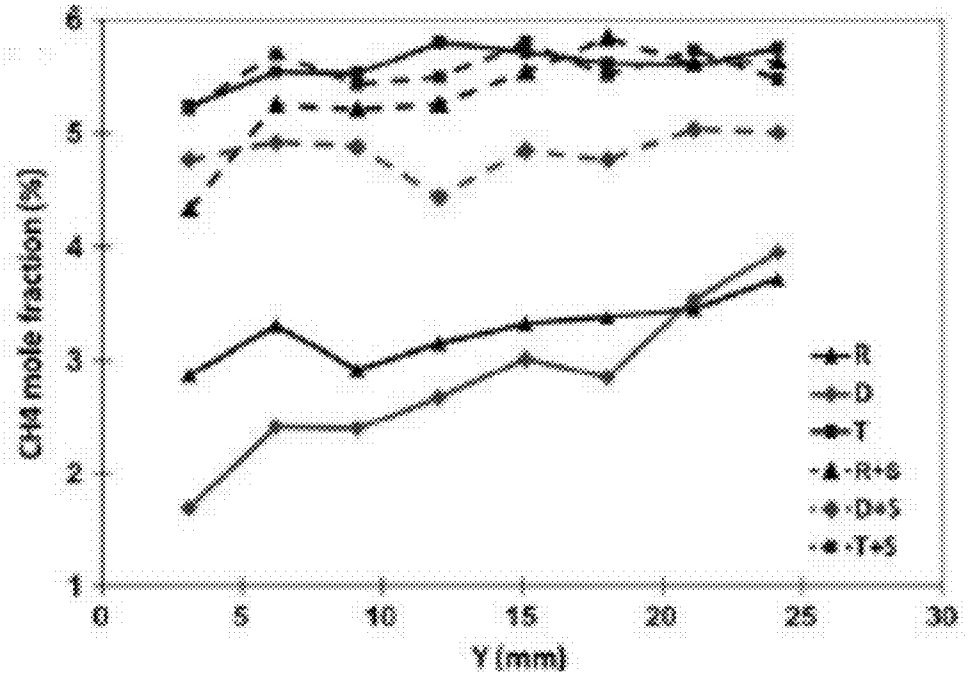
CH4 mole fraction (%)
Y (mm)
R
D
T
R+5
D+5
T+5

(a)

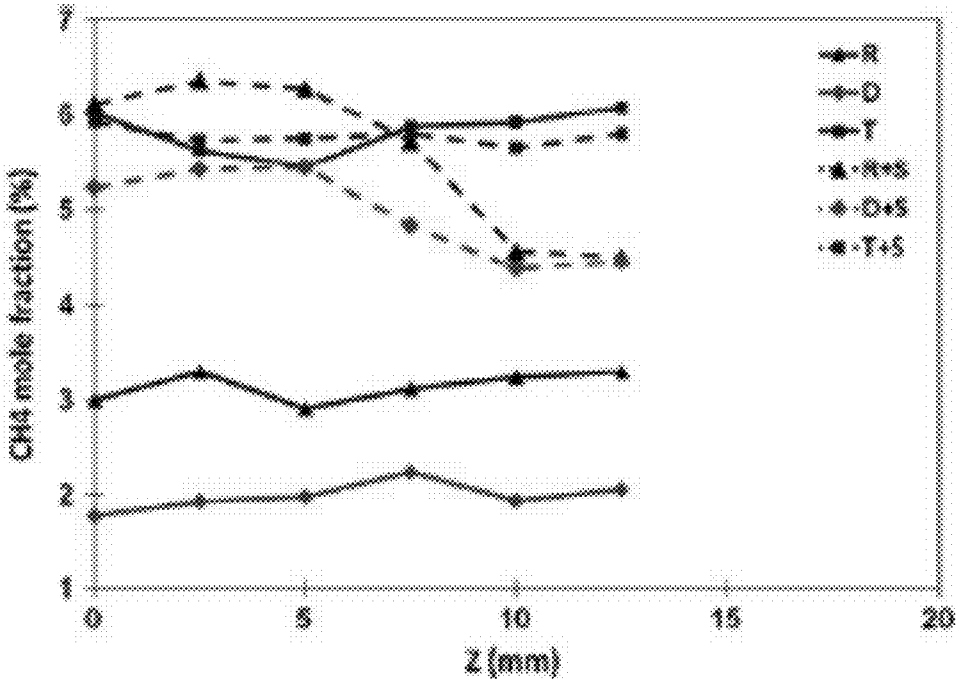
CH4 mole fraction (%)
Z (mm)
R
D
T
R+5
D+5
T+5

(b)

FIG. 7

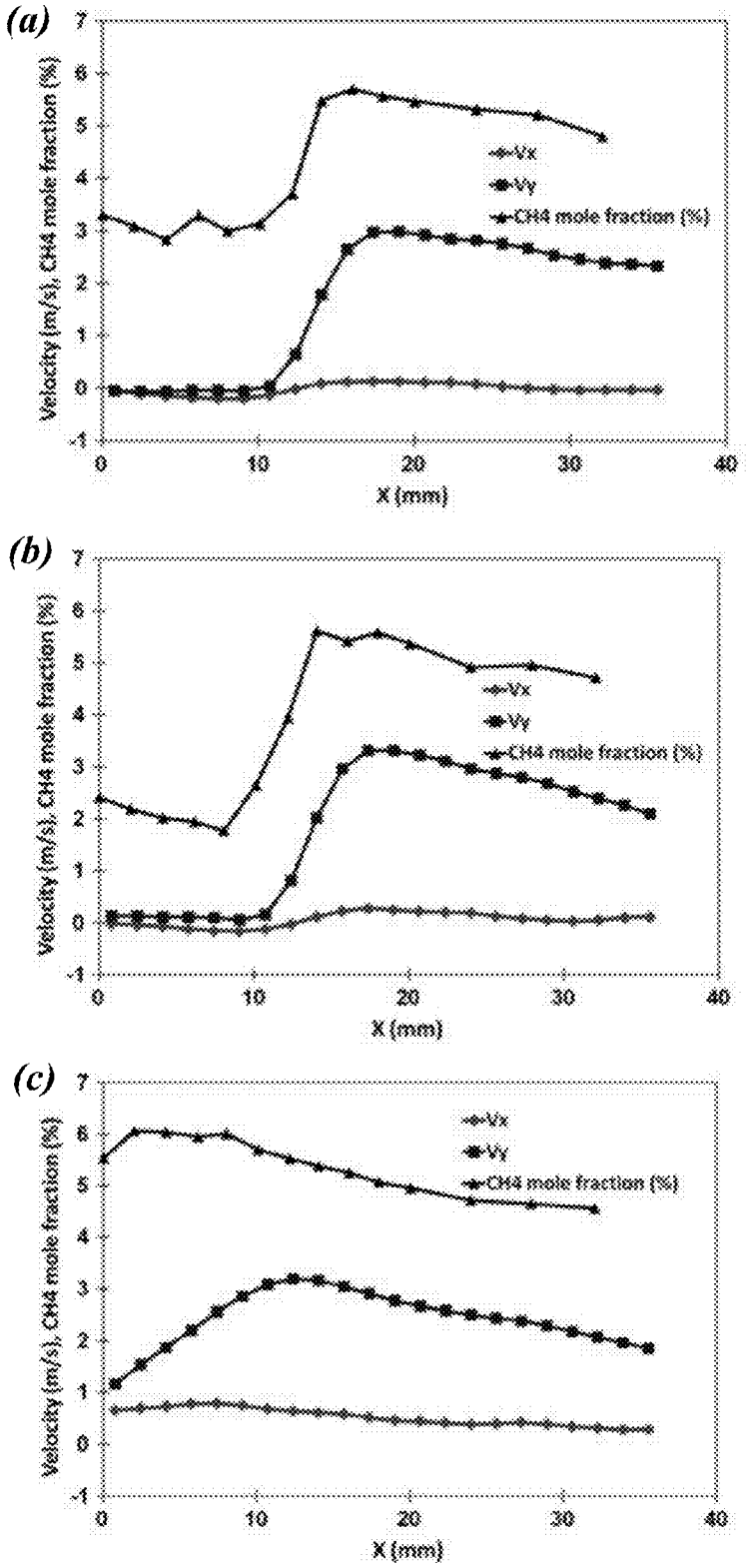
(a)
Velocity (m/s), CH4 mole fraction (%)
X (mm)
Vx
Vy
CH4 mole fraction (%)
(b)
Velocity (m/s), CH4 mole fraction (%)
X (mm)
Vx
Vy
CH4 mole fraction (%)
(c)
Velocity (m/s), CH4 mole fraction (%)
X (mm)
Vx
Vy
CH4 mole fraction (%)

FIG. 8

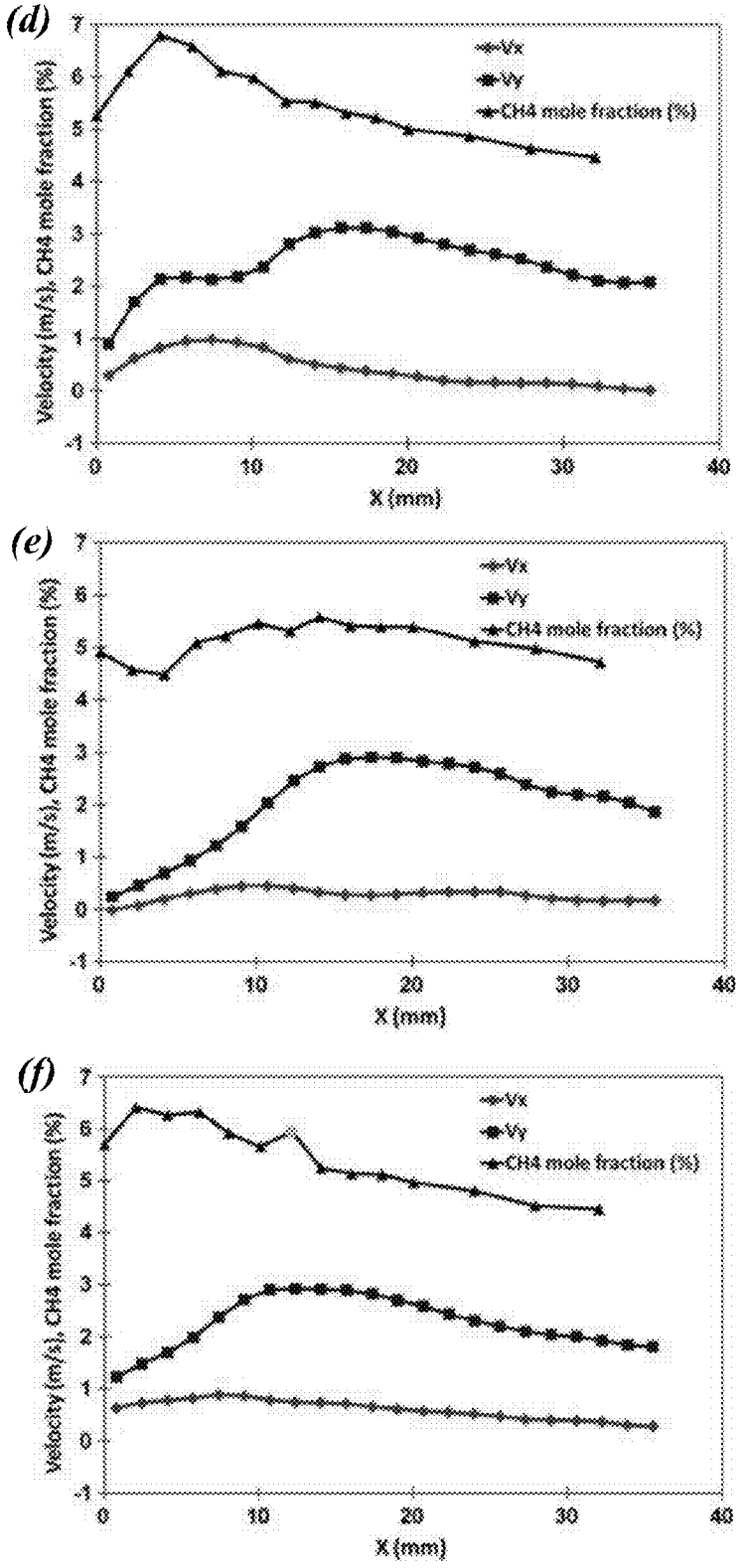
(d)
Vx
Vy
CH4 mole fraction (%)
Velocity (m/s), CH4 mole fraction (%)
X (mm)
(e)
Vx
Vy
CH4 mole fraction (%)
Velocity (m/s), CH4 mole fraction (%)
X (mm)
(f)
Vx
Vy
CH4 mole fraction (%)
Velocity (m/s), CH4 mole fraction (%)
X (mm)

FIG. 8 (cont.)

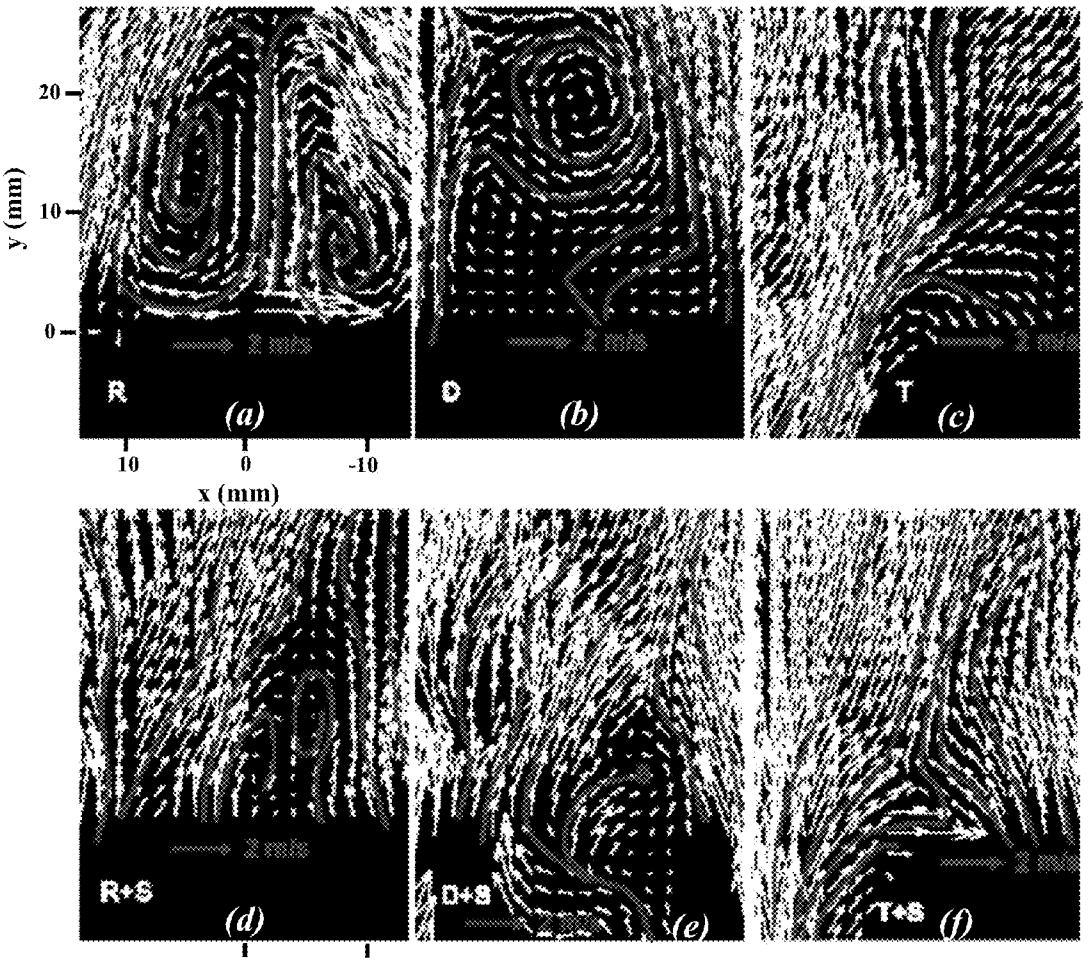

FIG. 9

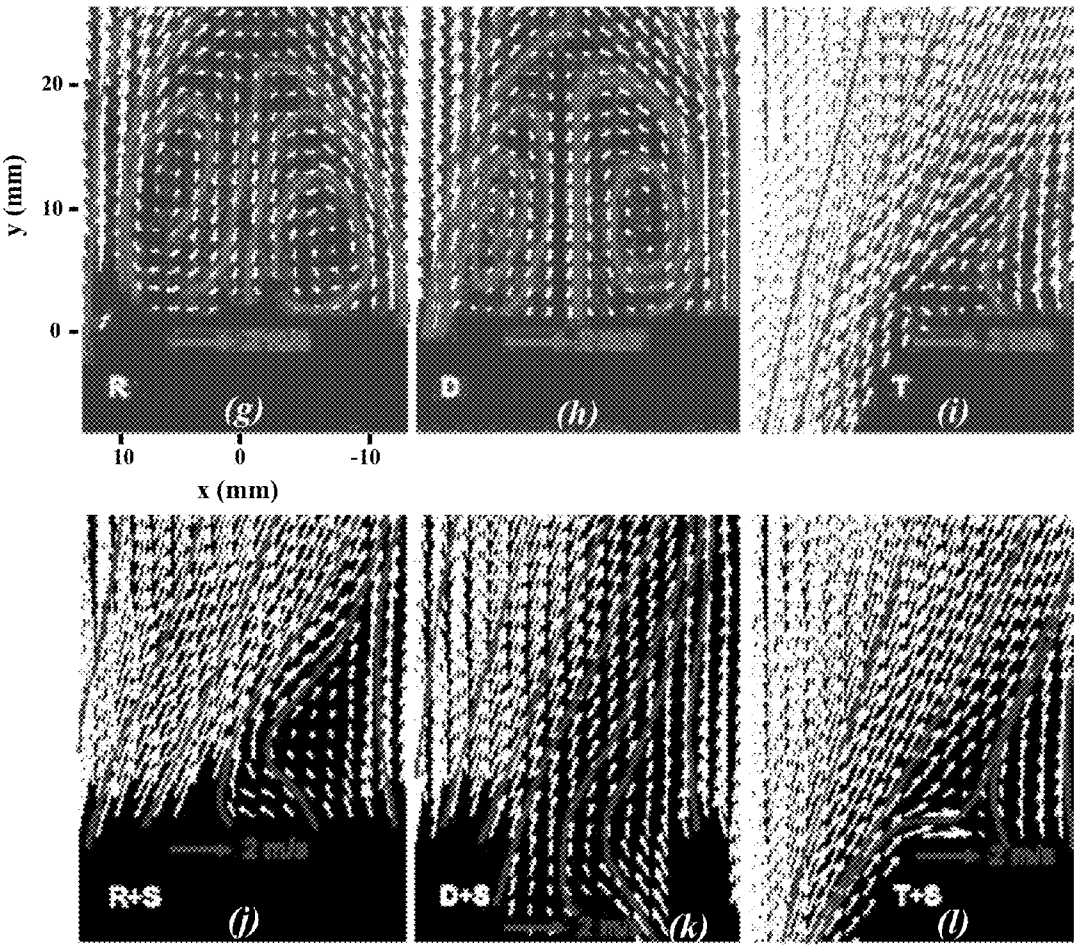

FIG. 9 (cont.)

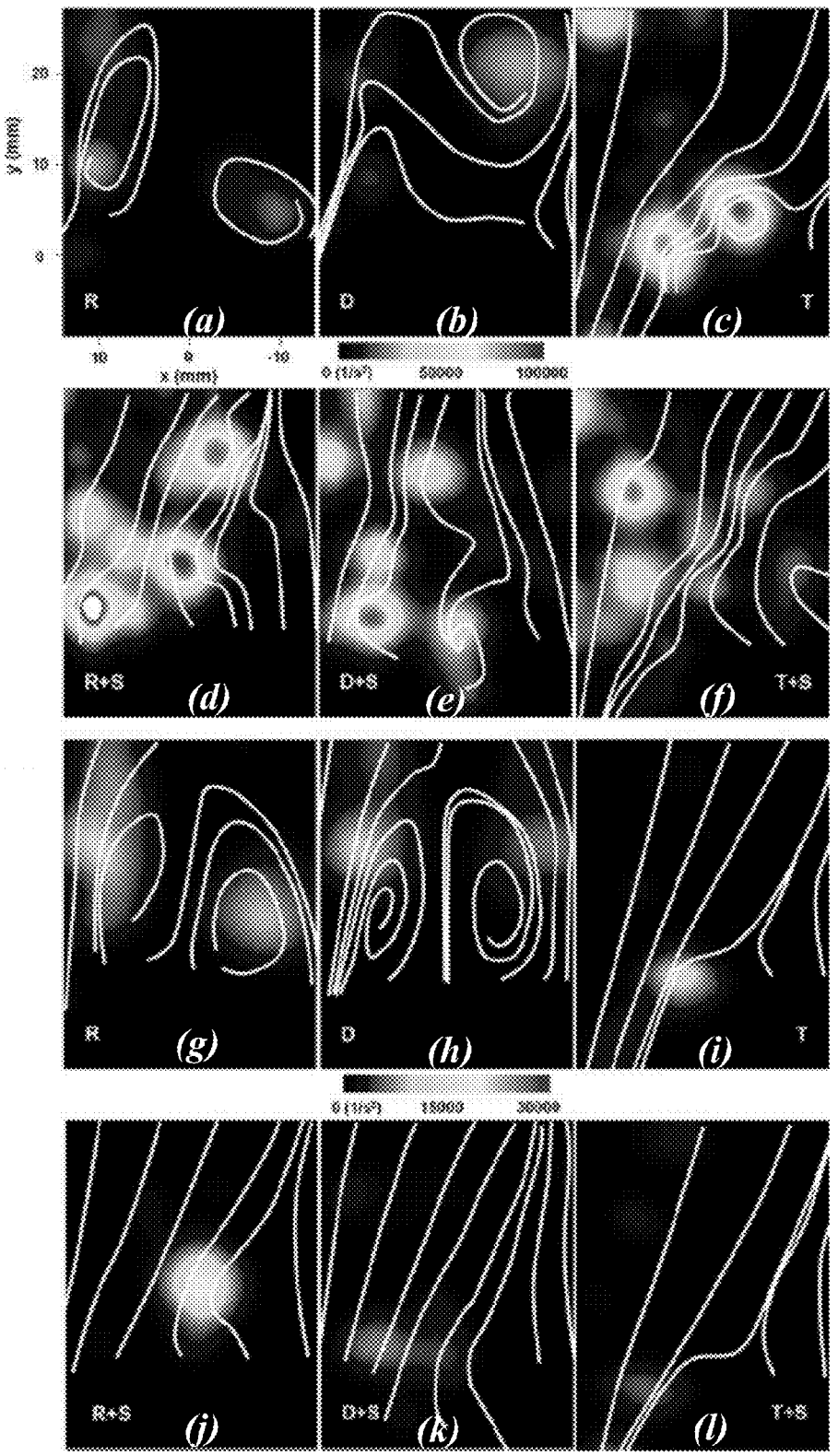
y (mm)
20
10
0
R
(a)
D
(b)
T
(c)
10
0
-10
x (mm)
0 (1/s²)
50000
100000
R+S
(d)
D+S
(e)
T+S
(f)
R
(g)
D
(h)
T
(i)
0 (1/s²)
15000
30000
R+S
(j)
D+S
(k)
T+S
(l)

FIG. 10

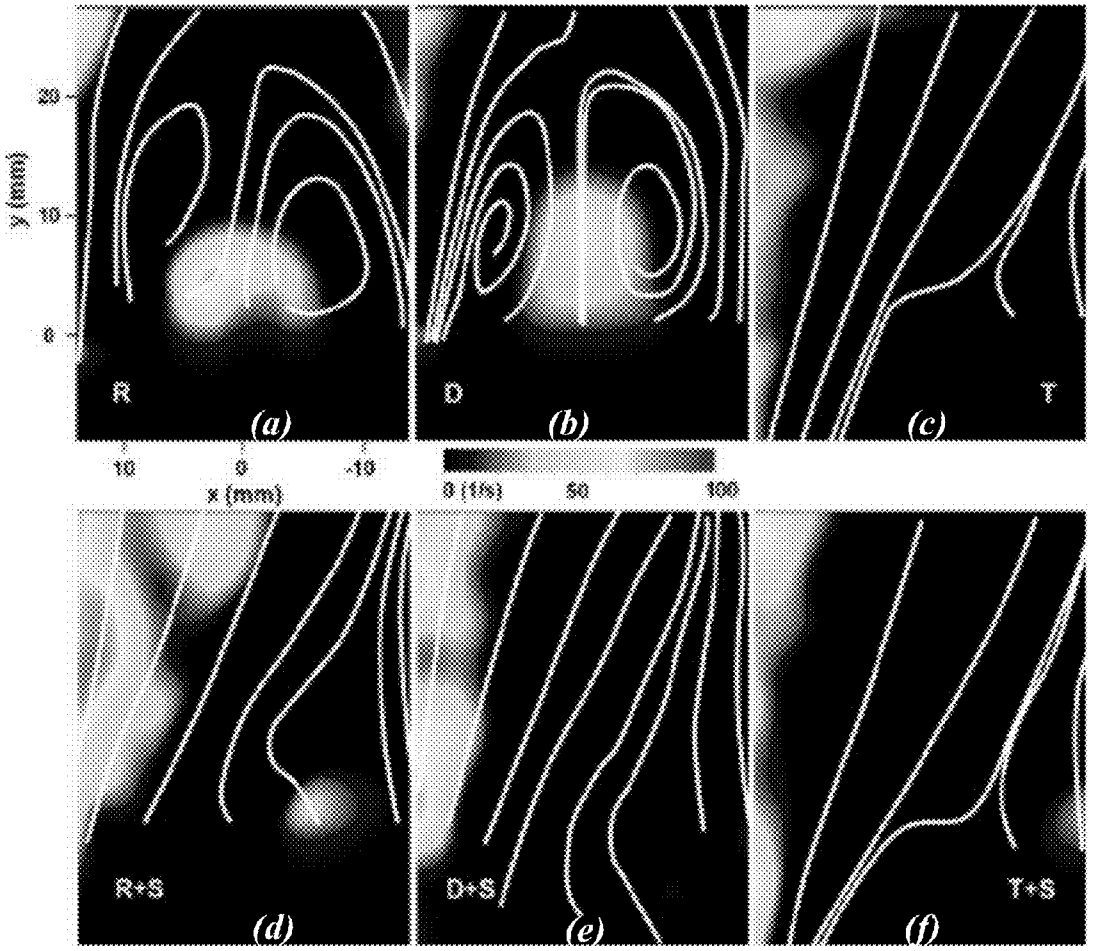

FIG. 11

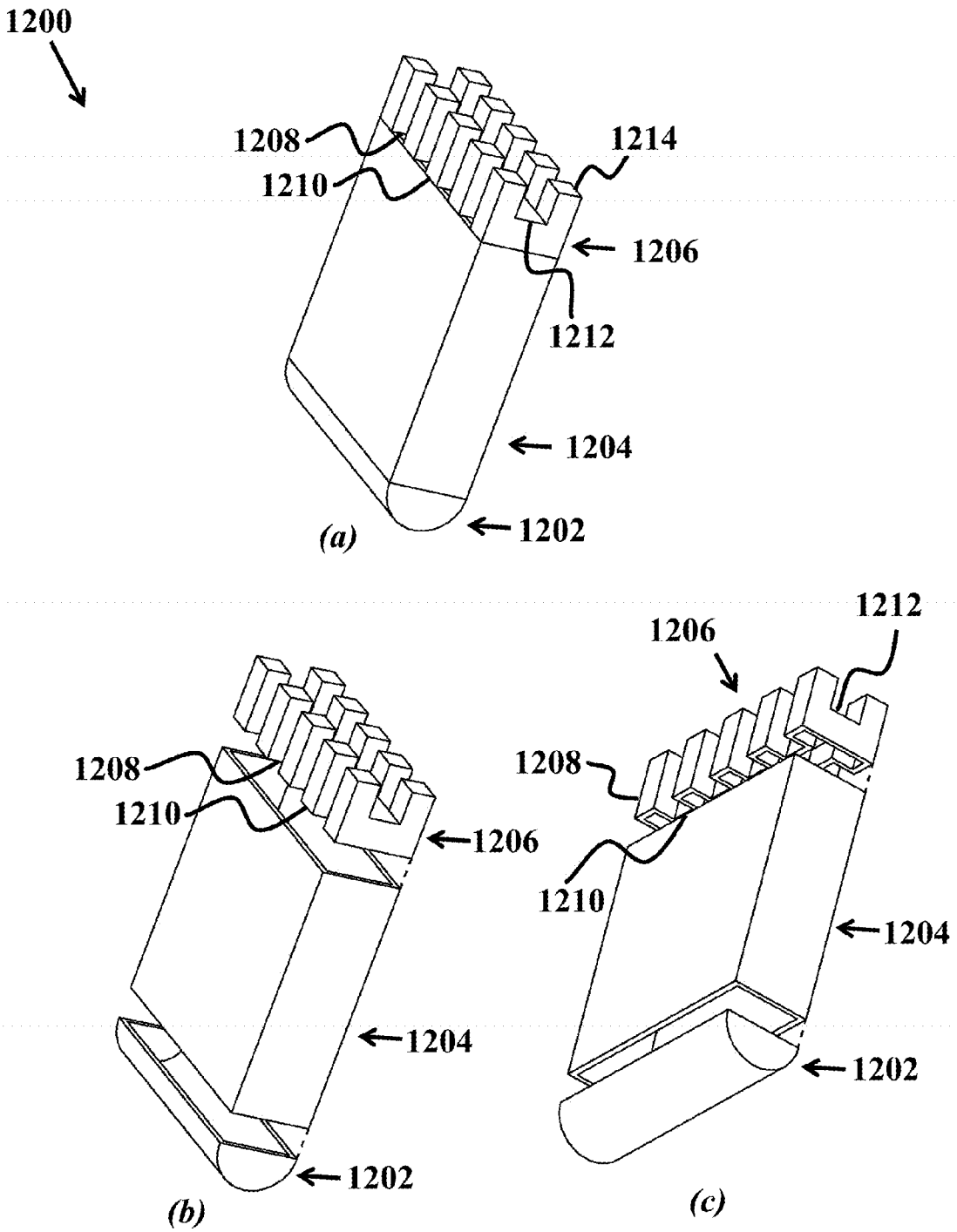
1200
1208
1210
1214
1206
1212
1204
1202
(a)
1208
1210
1206
1204
1202
(b)
1212
1206
1208
1210
1204
1202
(c)

FIG. 12

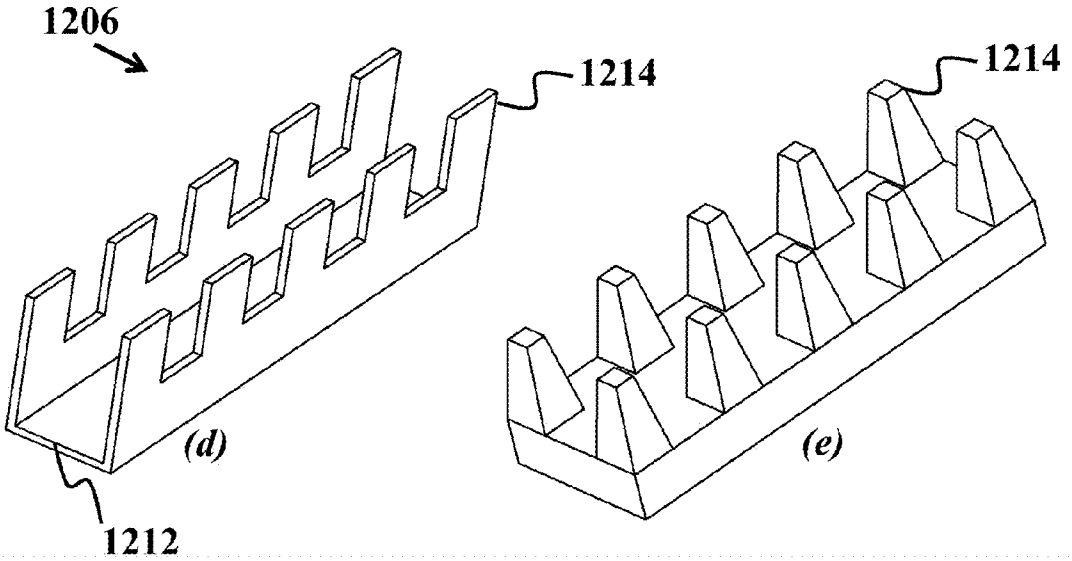
1206
1214
1214
(d)
(e)
1212

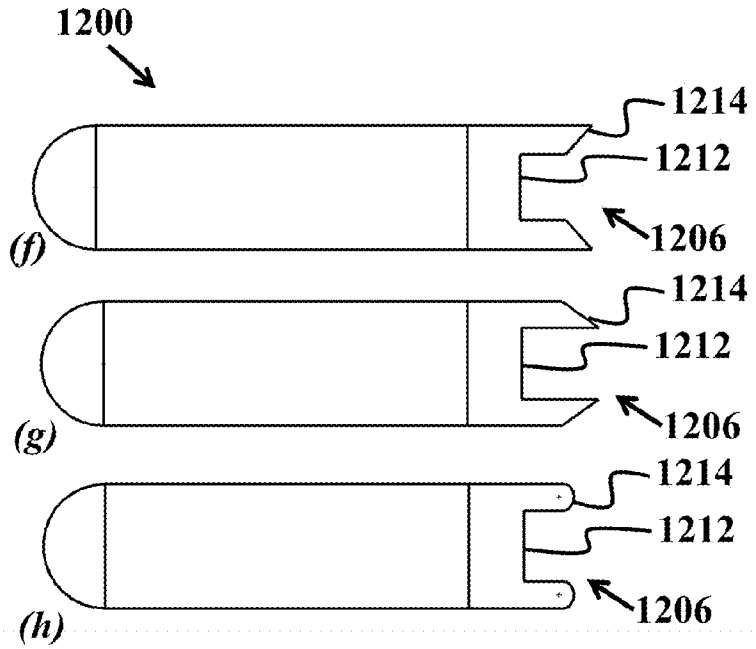
1200
1214
1212
1206
(f)
1214
1212
1206
(g)
1214
1212
1206
(h)

FIG. 12 (cont.)

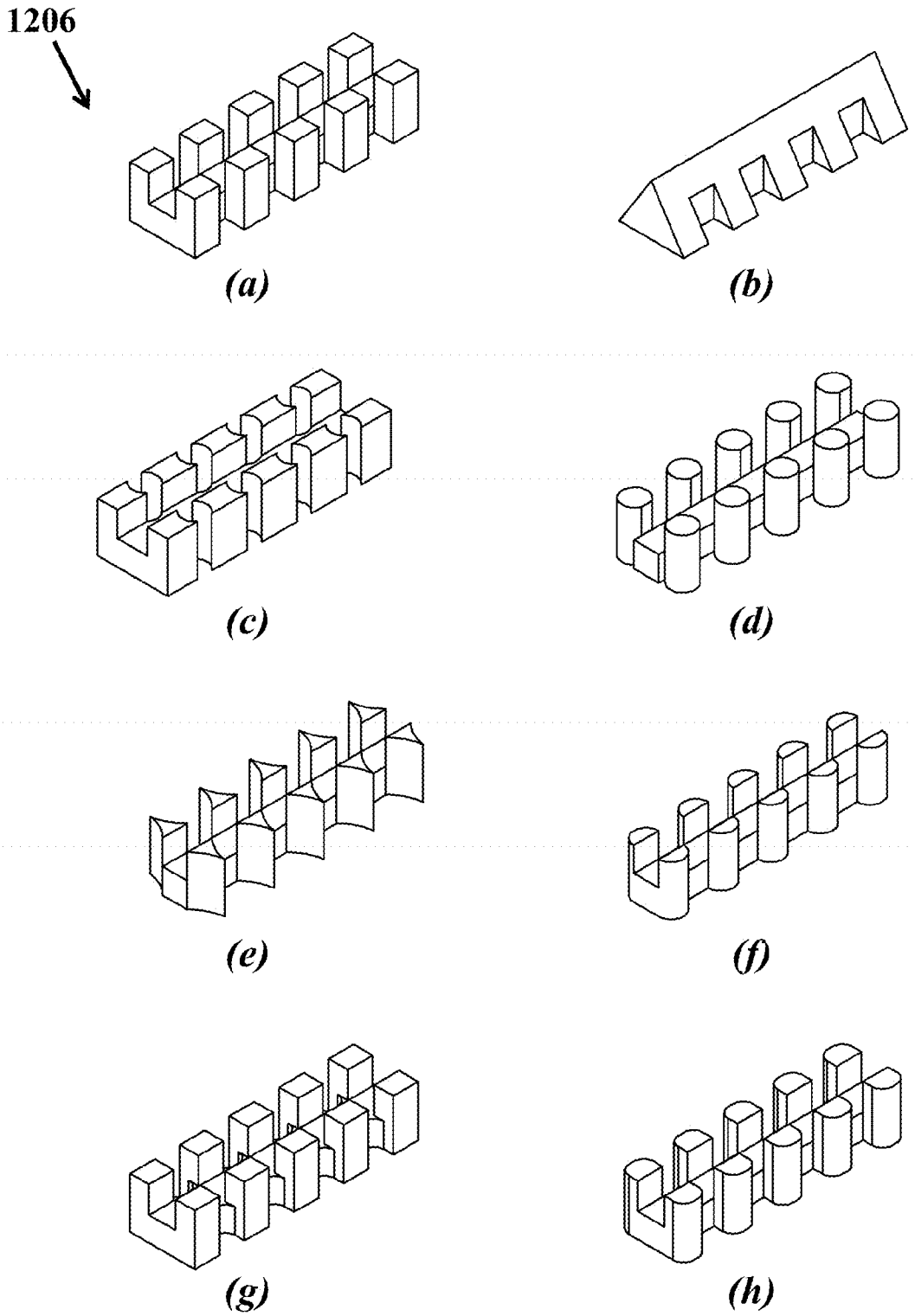

FIG. 13

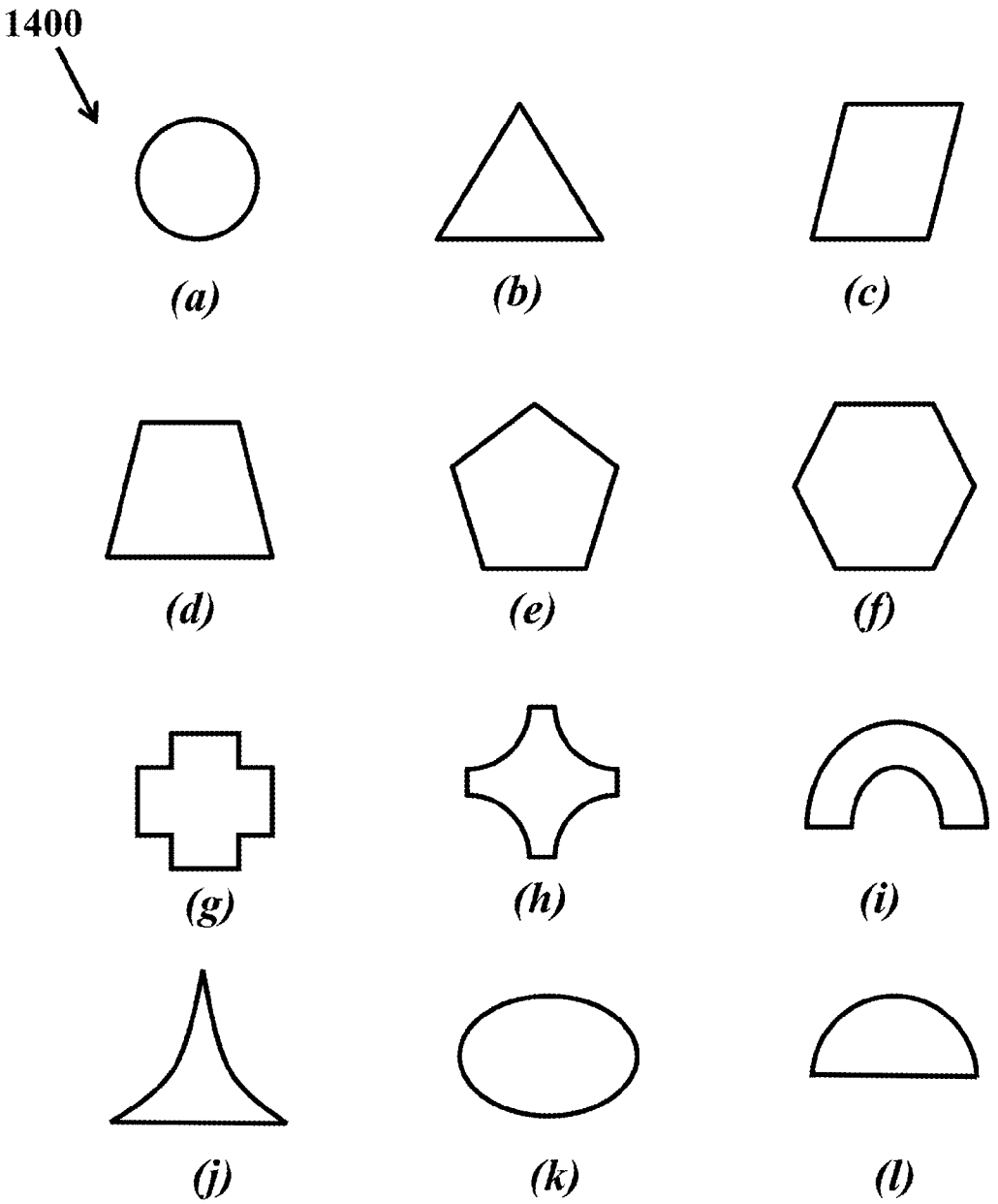

FIG. 14

METHOD AND APPARATUS FOR ENHANCED FLAMEHOLDING IN AUGMENTORS

CROSS-REFERENCE TO RELATED APPLICATIONS

[0001] This application is a continuation-in-part of U.S. patent application Ser. No. 12/806,958 filed Aug. 24, 2010, which is incorporated herein by reference. U.S. patent application Ser. No. 12/806,958 filed Aug. 24, 2010 claims benefit of U.S. Provisional Patent application 61/236,456 filed Aug. 24, 2009, which is incorporated herein by reference.

STATEMENT OF GOVERNMENT SPONSORED SUPPORT

[0002] This invention was made with Government support under contract FA9550-08-C-0039 awarded by U.S. Air Force. The Government has certain rights in this invention.

FIELD OF THE INVENTION

[0003] The current invention relates to jet engines. More particularly, the invention relates to jet engine flame holder bluffbodies.

BACKGROUND OF THE INVENTION

[0004] The lean blowout limit of bluffbody flames has been studied extensively for several decades since the improvement of flame stability in the lean environment is a primary purpose for using bluffbodies in various practical combustion devices such as industrial burners and boilers, furnaces, and thrust augmentors. It is believed that the sequence of flame blowout in a fully premixed system that is stabilized by a bluffbody occurs in the following steps: (1) sporadic, local flame extinction, which produces "holes" in the flame, (2) more frequent appearance of the holes with approaching blowout, which eventually induces, (3) significant flame undulation with the appearance of a large-scale wake, and (4) the onset of blowout.

[0005] At stoichiometric equivalence ratios of the fully premixed system, the bluffbody flame exhibits little large-scale wake oscillation, while at lean blowout, the system exhibits considerable large-scale wake oscillation, so it remains unclear whether the presence of the large-scale wake oscillation has direct causality with flame blowout since both occur simultaneously as the fully premixed system is leaned out. It is believed that an alternate possibility is that at high heat release (e.g., stoichiometric operation) the flow stability is dominated by "outer modes" that imply little large-scale oscillation, and at low heat release (e.g., near blowout) the flow stability reverts to "central" oscillatory modes, so that the oscillatory motion does not necessarily dictate blowout but is merely a consequence of the lower heat release state at blowout.

[0006] These ideas are consistent with a prediction that a transition from outer modes to central modes when the ratio of burnt to unburnt gas temperatures is approximately four. The two phenomena are concomitantly observed whenever the bluffbody flame approaches blowout, and that the presence of an oscillatory wake can accelerate the flame blowout phenomenon by introducing a significant amount of low temperature fluid from the surroundings to the reaction zone such that the heat release from the chemical reactions (or rate of branching reactions) cannot keep up with the cooling effect due to the entrainment of cold gases (or rate of quenching reaction).

[0007] What is needed are geometrically modified bluffbody structures with a non-conventional geometry to generate mutually destructive incoherent vortices to assist in delaying the appearance of large-scale wake vortices.

SUMMARY OF THE INVENTION

[0008] To address the needs in the art, a jet engine flame holder bluffbody is provided that includes a leading edge that is rounded, a mid-body having a rectangular cross-section, and a trailing edge, where the trailing edge includes a rectangular cross-section having digitated cutouts from the rectangular cross-section, where the tailing edge projects upward according to a digitated cross-section, where material digits remain between consecutive pairs of the digitated cutouts.

[0009] According to one aspect of the invention, the trailing edge is a wedge-shape along a length of the trailing edge.

[0010] In a further aspect of the invention, the trailing edge is a block-shape along a length of the trailing edge. In one aspect, the trailing edge is a rectangular recess along an upper-center portion of the solid body, where each digit is a crenellation feature. In another aspect the crenellation feature has a cross-section that is square, rectangular, semi-circular, partly-circular, elliptical, or triangular. In one aspect the crenellation feature has a top surface that is angled towards a centerline along a length of the trailing edge, angled away from a centerline along a length of the trailing edge, or rounded. In another aspect the crenellation feature has tapered sidewalls.

[0011] According to another aspect of the invention, each digitated cutout includes a cross-section shape that is square, rectangular, semi-circular, partly-circular, elliptical, or triangular.

[0012] In yet another aspect of the invention, the material digits has a cross-section shape that can be square, rectangular, circular, semi-circular, partly-circular, elliptical, or triangular.

[0013] According to a further aspect of the invention, the leading edge is a hollow structure.

[0014] In another aspect of the invention, the mid-body is a hollow structure.

[0015] According to one aspect of the invention, the trailing edge is a hollow structure.

[0016] In a further aspect of the invention, the material digit is a triangular shape, where a side of the triangular shape is curved.

[0017] In yet another aspect of the invention, the trailing edge has a walled structure that is thin relative to a wall thickness of a hollow the mid-body.

BRIEF DESCRIPTION OF THE DRAWINGS

[0018] FIG. **1** shows an overall schematic of the experimental demonstration setup, according to one embodiment of the invention.

[0019] FIG. **2** shows a detailed schematic of the bluffbody, according to one embodiment of the invention.

[0020] FIGS. **3***a*-**3***f* show schematic drawings of various bluffbody bases. (**3***a*) R, (**3***b*) D, (**3***c*) T, (**3***d*) R+S, (**3***e*) D+S, (**3***f*) T+S, according to embodiments of the invention.

[0021] FIGS. **4***a*-**4***b* show blowout limits in terms of (**4***a*) local flow speed (measured at 2 cm side from methane nozzle)

and (**4***b*) equivalence ratio of fully premixed stream for various bluffbody base designs, according to embodiments of the invention.

[0022] FIG. **5** shows an Ozawa curve and a blowout data point in fully premixed mode with R base, according to one embodiment of the invention.

[0023] FIG. **6** shows the DeZubay correlation with data collected previously.

[0024] FIGS. **7***a*-**7***b* show methane mole fractions along (**7***a*) y and (**7***b*) z coordinates for the six modified geometries.

[0025] FIGS. **8***a*-**8***f* show methane mole fractions and velocity components (V_x and V_y) along x coordinate for the six geometries, according to embodiments of the current invention.

[0026] FIGS. **9***a*-**9***l* show instantaneous and ensemble averaged PIV images of the R, D, T, R+S, D+S, T+S geometries, according to embodiments of the current invention.

[0027] FIGS. **10***a*-**10***l* show swirling strength of instantaneous and ensemble averaged velocity fields of the R, D, T, R+S, D+S, T+S, according to embodiments of the current invention.

[0028] FIGS. **11***a*-**11***f* show strain rates of the averaged velocity field in the six example test geometry cases R, D, T, R+S, D+S, T+S, according to embodiments of the current invention.

[0029] FIGS. **12***a*-**12***h* show a jet engine flame holder bluffbody elements that include a rounded leading edge, a midbody having a rectangular cross-section, and a crenellation-featured trailing edge, according to embodiments of the invention.

[0030] FIGS. **13***a*-**13***h* show trailing edge geometries, according to different embodiments of the invention.

[0031] FIGS. **14***a*-**14***l* show features that represent exemplary cutout, material digit or crenellation cross-sections, according to embodiments of the invention.

DETAILED DESCRIPTION

[0032] The current invention provides an improvement of the lean blowout limit of bluffbody stabilized flames. The flame configuration includes a hybrid of partially and fully premixed flames, which is demonstrated by injecting methane jets from a streamline-shaped bluffbody into a fully premixed methane/air crossflow. According to the invention geometric configurations of the bluffbody include a base that has two-dimensionally modified geometries and three-dimensional local cavities. According to one embodiment, the blowout limit of a hybrid configuration is extended by up to 12% (in terms of the equivalence ratio of the crossflow). Gas chromatographic sampling and particle image velocimetry (PIV) show that high fuel mole fraction regions coexist with regions of low speed flow for the modified geometries. Further, PIV analysis shows that the downstream flow fields of the modified bases generally have a larger number of incoherent vortices and lower strain rate in comparison with those of the unmodified base.

[0033] In accordance with the current invention, three flame configurations are presented. The first is a fully premixed freestream stabilized by a bluffbody ("fully premixed mode"); the second is an air freestream in which fuel is discharged from the bluffbody ("partially premixed mode"); and the third is a combination of these two, namely a fully premixed freestream with additional fuel discharged from the bluffbody "hybrid mode". For this hybrid mode, a small amount of fuel injection is effective in enhancing stability of bluffbody stabilized flames, e.g., extending the lean blowout limit.

[0034] As presented below, the blowout limit of the flame can be extended with local cavities in the hybrid mode, according to one embodiment of the current invention. The blowout extension is not observed when the flame configuration is solely in the partially or fully premixed mode. In addition, it is shown that high local fuel mole fraction in low speed flow regions observed in the local cavity geometries is primarily attributed to the extension of flame stability in the hybrid mode.

[0035] These results are validated by gas chromatographic sampling and particle image velocimetry (PIV) measurements. Finally, the swirling strength and strain rate fields in the vicinity of the bluffbody bases are provided to compare the change in the flow field in the presence of local cavities.

[0036] As shown in FIG. **1**, the experimental setup includes five parts: (1) a main gas blower to provide a fully premixed fuel/air stream in the vicinity of a bluffbody, (2) a bluffbody through which methane fuel is injected to form jets in crossflow with the room temperature premixed stream, (3) turbulent grids with multiple slots (for additional air injection) to mimic higher Reynolds number flow, (4) a PIV system to measure the local freestream speed and the velocity fields in the vicinity of the bluffbody, and (5) a gas chromatography and sampling system to investigate the concentration field downstream of the bluffbody.

[0037] The main gas blower, which provides the required freestream flow, was originally designed as a premixed burner, but is used here for providing a room temperature, fully premixed stream in the current study, and is located centrally in a 50 cm×50 cm cross-sectional area vertical wind tunnel which can generate ~3.5 m/s flow. The burner face has 2,184, 1/16-inchdiameter holes on the top surface whose overall diameter is 8.27 inch such that a uniform fully premixed flow can be generated over a relatively wide region. To make the fully premixed stream, air is delivered by a 1.5-hp air blower and mixed with methane ~3 m upstream of the top surface of the gas blower. The pressure drop across the perforated top plate is measured to determine the mass flowrate; the velocity is proportional to the square root of the pressure drop. The equivalence ratio of this (fully premixed) main stream is used, which varies from 0.54 to 0.72 (confirmed by gas chromatographic measurement), as a criterion to determine the blowout limit. It should be noted that the local flow speed in the vicinity of the bluffbody base is varied, which is the second blowout criterion used in the current exemplary experimental demonstration of the invention. The variation is achieved by injecting additional air from the turbulent grid located ~1.5 inch downstream of the perforated burner surface while the flow speed generated from the main blower is kept fixed as 0.83 m/s.

[0038] FIG. **2** shows a basic geometry of a bluffbody having a 4.5-inch-long, 1-inch-thick, and 6-inch-wide rectangular body with a ½-inch-radius rounded nose. For choice of material, a porous ceramic (fused silica, 63% nominal porosity) was selected. The methane is delivered through a ⅜-inch OD stainless steel tube to produce two sets of opposing jets in crossflow. To guide the jet direction normal to the freestream flow, six ⅛-inch OD tubes (⅛ inch length, three on each side) are welded to the main tube. The three nozzles on each side are located ½ inch upstream of the base of the bluffbody with 1 inch spacing.

[0039] The speed of the methane jet is kept fixed at ~1.4 m/s throughout this example. Also shown in FIG. **2** are the x, y, and z axes with the origin located 1 inch downstream of the physical base as shown. The dotted region is filled with various geometrically modified bluffbody bases, namely Reference or R, D, T, R+S, D+S and T+S, as shown in FIGS. **3***a*-**3***f*. R is a solid rectangular bar and serves as a reference; D is a geometry that has a lateral cavity (0.5 inch width and 0.3 inch depth) on the R; T is a solid bar that has a triangular cross section; R+S is a geometry that has spanwise local cavities (pass-through cavity with 0.5 inch width and 0.4 inch depth) on the R; D+S is a geometry that has S cuts on the D geometry while T+S has S cuts on the T geometry. While all geometries tested here have identical height (1 inch), it is noteworthy that they can be grouped as non-S cavity bases (R, D, and T) and S cavity bases (R+S, D+S, and T+S). Showing the role of the S cavity is also a primary purpose of the current exemplary demonstration.

[0040] The turbulence grid is placed ~1.5 inch downstream from the top surface of the perforated plate. It is composed of two, top and bottom, layers of ½ inch OD, 8-inch-long ceramic (99.9% Al2O3) hollow tube arrays (see FIG. **2**). Each array is formed by 6 parallel-placed ceramic tubes with 1.25 inch inter-distance (36% open area). The top and bottom arrays are placed perpendicular each other such that the shape of the open area becomes square. Because of the grid, the freestream turbulent fluctuation can be increased from ~5% (with no grid) to 8% (with the grid). There are five 1 mm×3 mm sized slots (whose inter-distance is ~1 inch) on the top surface of each top-layered ceramic tube for additional air injection in the parallel direction of the main flow. The amount of the air injection typically varies from 40 to 200 SLPM. The overall flow speed (produced from the main gas blower and the additional air injection) measured in the vicinity of bluffbody at the methane nozzle (~2 cm away from the nozzle along the x direction) typically ranges from 1.2 to 5.6 m/s. It is presumed that the air injected through the slots of the ceramic tubes is well mixed with the main stream in the region of interest that is adjacent to the base of the bluffbody, 165 D (D: slot width (1 mm)) downstream of the air jets. This is confirmed by uniform particle distribution in the region in the presence of the unseeded air jets with the seeded main stream.

[0041] For the PIV studies, ~100 mJ/pulse (532 nm), double pulsed Nd:YAG laser (New Wave, Gemini PIV) with ~0.5 mm sheet thickness is used for illuminating 3-μm-nominal diameter Al_2O_3 particles seeded into the flow. The Al_2O_3 particles are mixed in the main premixed stream such that adequate seeding density could be achieved. The resulting Mie scattering is detected by a double exposure CCD cameras (La Vision, Flow Master).

[0042] Gas chromatographic measurements were taken for quantifying the local methane concentration in the vicinity of the bluffbody base via a Varian 3400 Gas Chromatograph equipped with Porapak Q (for nitrogen and oxygen) and Molecular sieve 5A (for methane) as columns and a thermal conductivity detector (TCD). All sampling measurements are taken in the absence of flame. For the sampling, the spatial scanning is carried out by three translation stages (along the x, y, and z coordinates) using a ~1-mm diameter (ID), 200-mm-long stainless steel probe.

[0043] Regarding the extension of blowout limits in the presence of local (S) cavity, FIG. **4***a* shows the result of ensemble averaged flame blowout limit in terms of local flow speed measured at a 2 cm distance away from the methane nozzle in each of the six cases discussed above, under hybrid, fully premixed, and partially premixed conditions. To vary the local flow speed, additional air was injected from the turbulent grid and adjusted its flowrate (from 40 to 200 SLPM: 1.2-5.6 m/s freestream velocity, 0.6-0.1 equivalence ratio of the freestream) until the entire bluffbody stabilized flame, resulting from the fully premixed flow from the gas blower and the pure methane jet injected from the methane nozzle, is blown out. The equivalence ratio and the speed of fully premixed stream from the gas blower are kept identical at 0.72 and ~0.83 m/s, respectively. The amount of methane injection from the nozzle was also kept fixed at ~3 SLPM such that the (nominal) square root of the momentum ratio (r) calculated from the main fully premixed stream and the injected methane was ~1.2 (note that the r ranges 0.2-0.9 when it is calculated based on the nominal local speed formed by the main fully premixed flow and additional air injection). The relative placement of the methane nozzle and the local cavity is in-phase, i.e., the nozzle exit is aligned with the centerline of local cavity.

[0044] FIGS. **4***a*-**4***b* show blowout limits in terms of a local flow speed (measured at 2 cm side from methane nozzle) and b equivalence ratio of fully premixed stream for various bluffbody base designs. For FIG. **4***a* the equivalence ratio of the fully premixed stream is kept fixed as 0.72 (for fully premixed and hybrid modes) while nominal local flow speeds of FIG. **4***b* are also kept identical to 1.5 m/s (fully premixed mode) and 2.8 m/s (hybrid mode). In FIG. **4***a*, it is shown that the critical nominal flow speeds (black solid bar) where blowout occurs are as low as ~3.7±0.1 m/s (R), ~3.7±0.1 m/s (D), and ~4.7±0.2 m/s (T) for the non-cavity geometries. The improvements of the critical speeds observed by adding local cavities on the original geometries are apparent: by 48% for R+S geometry, by 42% for the D+S, and by 10% for the T+S geometries. The smallest difference observed in the T and T+S geometry is probably due to the fact that (1) the T geometry already shows a good capability to extend the blowout limit in comparison with those of R and D and (2) the size of the S cavity on the T geometry is small (due to slanted side surface of T) such that the effect of added S cavity is relatively weaker. Here, it is noteworthy that the identical experiments without the injection of pure methane (fully premixed mode) illustrated in the shaded bars of FIG. **4***a* show no apparent stability enhancement with the S cavity addition.

[0045] This observation is consistent with previous results, where there is a minimal positive effect on blowout limit extension with a geometrical change in the bluffbody. For comparison, similar experiment was carried out but with methane injection into pure air crossflow (partially premixed mode).

[0046] As shown in the dotted bar, no significant extension of blowout limit is observed among the various geometries. It is believed that this observation with the partially premixed mode (no appreciable cavity effect) is primarily due to the limited amount of the pilot fuel injected via the fuel jets on the bluffbody that is too small to sustain largescale flames. However, the cavity entrained jet fuel is capable of enhancing flame stability in the presence of the fuel containing freestream in the hybrid mode.

[0047] For the case of the fully premixed mode, an Ozawa curve that correlates blowout limits of premixed subsonic flames to Damkohler number is used for validation of the blowout limit observed in the current example (FIG. **5**). The Ozawa curve is defined by the following equation:

$$Da=\exp[8.75(\phi-1)^2]$$

where Da and ϕ are the Damkohler number and the equivalence ratio, respectively. Also, a simple representation of the Damkohler number is defined as follows:

$$Da=\frac{H/U_o}{\left(\frac{\alpha}{S_L^2}\right)\left(\frac{1\text{ atm}}{p}\right)^n\left(\frac{300\text{ K}}{T}\right)^m}$$

where H, Uo, α, S_L, p and T are the bluffbody thickness (1 inch), freestream velocity (1.7 m/s, blowout velocity of R base in fully premixed mode), thermal diffusivity, maximum laminar burning velocity, pressure, and temperature of the freestream, respectively. A value of thermal diffusivity presented in a literature was used here, which is 0.213 cm^2/s for a lean CH_4/air mixture at room temperature and 1 atm, and the laminar burning velocity of a methane/air mixture of equivalence ratio 0.5 at 1 atm is approximately 10 cm/s.

[0048] The calculated Damkohler number for the R base at the blowout limit (q Da_{bo}) in the fully premixed mode is approximately 7 ($1/Da_{bo}$=0.14). The data point (0.5 equivalence ratio at $1/Da_{bo}$=0.14) is indicated (black dot) in the graph (FIG. **5**) and is very close to the Ozawa curve.

[0049] Alternatively, another measure of blowout (dimensionless DeZubay parameter) is employed to confirm the above observation.

$$Dz=\frac{10{,}000\cdot U}{p^{0.95}T^{1.2}L^{0.85}}$$

where Dz, U, p, T, and L are the modified DeZubay parameter, flow velocity (ft/s), pressure (psi), temperature (° R), and the half bluffbody thickness (0.5 inch), respectively. The modified DeZubay parameters corresponding to the flow velocities of the current exemplary demonstration of the invention (1.5 and 2 m/s) are 2.1 and 2.9 (equivalence ratio ranges between 0.55 and 0.4), respectively. FIG. **6** shows the flame blowout equivalence ratio as a function of the modified DeZubay parameter measured by various researchers. The results of the current example are located in the lower left corner of the equivalence ratio-Dz space.

[0050] In FIG. **4***b*, the blowout limits in terms of equivalence ratio (of the fully premixed main stream) in each of the six geometries are plotted. For this example experiment, the amounts of injected air (from the turbulent grid) are kept fixed at ~50 SLPM (in the fully premixed case) and ~100 SLPM (in the hybrid case), respectively. The blowout limit is measured by decreasing the amount of methane in the fully premixed stream until no bluffbody stabilized flame is present, while the air flowrate of the stream is kept identical at ~1,720 SLPM.

[0051] The resulting nominal flow speeds of the stream are 1.5 m/s (fully premixed mode) and 2.8 m/s (hybrid mode). In the hybrid mode (black solid bar), it is shown that the presence of the local cavity in the R+S, D+S, and T+S geometries extends the blowout limit from 0.62±0.02 (R and D) and 0.61±0.02 (T) to 0.55±0.02 (R+S), 0.56±0.02 (D+S), and 0.58±0.02 (T+S).

[0052] This trend is consistent with what was observed in FIG. **4***a*. Again, for the fully premixed mode (shaded bar), no significant dependence of the blowout limits on the geometries tested is observed, which also confirms the previous observation in FIG. **4***a*. Thus, FIG. **4***a* and FIG. **4***b* suggest that there are no clear benefits to blowout limits in both the fully premixed and partially premixed modes of operation but clear benefits in the hybrid mode of operation. Based upon these results, it is believed that the presence of large-scale oscillations, presumably influenced by the geometric modification of the bluffbody, is not a fundamental determinant of blowout since it appears not to be affected by the S-modifications (which act to eliminate or minimize large-scale oscillations), and that this phenomenon is more likely related to the observations discussed above. In other words, if the augmentor operates at $T_{burnt}/T_{unburnt}$<~4, i.e., a lean condition, oscillatory modes are dominant, but if such modes are destroyed by geometrical modifications, no improvement in stability is achieved. Thus, the oscillatory motions cannot be the dominant cause of blowout.

[0053] The different blowout dependence on the geometric modification observed in the hybrid and the fully premixed modes show that the way of interaction between the small pure methane stream (namely, partially premixed stream) and the local cavities are a key aspect of the observed blowout limit extension. In this context, the variation in the mole fraction and the flow fields in the vicinity of the six base geometries is of interest. Thus, in the following sections, the measurements of temporally averaged mole fraction/flow fields using gas chromatographic sampling and particle image velocimetry (PIV) will be presented.

[0054] Regarding the fuel mole fraction field in the vicinity of the base FIG. **6** and FIG. **7***a* show the variation in methane mole fraction along y and z coordinates in the non-burning hybrid mode case, respectively. For all these mole fraction measurements, the equivalence ratio and the speed of the fully premixed stream were kept fixed as 0.72 and 0.83 m/s, respectively. The flowrate of additional air injection is also invariant at 100 SLPM (2.8 m/s freestream flow), and the resulting speed including the air injection (measured at x~20 mm) is ~3 m/s. The measurements in FIG. **7***a* were taken at x=0 mm, i.e., the center of bluffbody in the xy plane, and z=0 mm, i.e., the center of local cavity in the yz plane. The measurements in FIG. **7***b* are taken at x=8 mm and y=6.5 mm, i.e., 6.5 mm from the top surface of the bluffbody.

[0055] Along the y coordinate (FIG. **7***a*), the methane mole fractions of non-local cavity geometries, especially R and D, are generally lower by ~50% in comparison with those of local cavity geometries (R+S, D+S, and T+S) at least up to y=1D, where D is the width of the bluffbody (1 inch). It is believe that the high fuel mole fractions, especially in the vicinity of base, are an important feature of local cavity geometries for increasing flame stability. It is expected that the most active interactions between the base geometry and the flow will occur in this region. From this result, it appears that the presence of the local cavity prevents the pure methane stream from being excessively diluted such that the partially premixed stream can effectively pilot the fully premixed stream. It is noteworthy that the T geometry shows a mole fraction field as high as those of local cavity geometries.

[0056] This high mole fraction can be also expected from PIV results for the geometry (see later FIG. **9** for the detailed flow field), which indicates the presence of skewed flow along the slanted side surface of the T geometry. It is believed that the skewed flow can effectively deliver the pure methane

stream, especially at this low value of r (r~1), to the region investigated here such that overall fuel mixture fraction in that region remains high.

[0057] FIGS. **7***a*-**7***b* show methane mole fractions along y and z coordinates for the six modified geometries. The equivalence ratio of fully premixed stream is kept fixed as 0.72. The flowrate of additional air injection is also invariant as 100 SLPM such that the resulting nominal flow speed measured at 2 cm side from methane nozzle is ~3 m/s. Measurement locations are x=0 and z=0 for FIG. **7***a*, and x=8 mm and y=6.5 mm for FIG. **7***b*.

[0058] FIG. **7***b* shows the result of the same experiment but along the z coordinate. One can observe from the figure that a similar trend exists as in the previous observations: approximately two times higher local fuel mole fraction for the local cavity geometries (and T geometry) in comparison with non-local cavity geometries (especially R and D). It is noted, however, that the mole fractions of R+S (triangle dotted line) and D+S (diamond dotted line) decrease with increasing z, while the other four geometries show a relatively invariant trend of mole fraction along the z coordinate. The decay is more apparent when z is greater than ~6 mm. This is because the local cavity section ends and the wall section starts from z=6.4 mm in those two geometries, which confirms that the local cavity acts as an effective conduit of less diluted fuels. To further study the capability of the local cavity placement relative to the methane jet to localize the fuel stream, the blowout limit dependence was briefly investigated (under the experimental conditions to those of FIGS. **7***a*-**7***b*) on the location of the cavity relative to the methane jet nozzles. The result shows that the blowout limit for out-of-phase placement (i.e., the case that the center of the wall section is aligned with the methane nozzle) is ~20% (in terms of local flow speed) or ~7% (in terms of equivalence ratio of fully premixed stream) worse than those of in-phase placement (i.e., the case where the center of the cavity section is aligned with the methane nozzle) for both R+S and D+S geometries.

[0059] Comparing simultaneously the mole fraction and velocity fields is of interest. This is because when considering that the total amount of fuel injection is the same for every geometry investigated, one can find that the result shown in FIGS. **7***a*-**7***b*, e.g., the lower methane mole fraction for non-local cavity geometries, implies that there should also exist a region of higher mole fraction in those geometries. In this context, the modes of distribution of the fuel mole fraction in a flow field are likely more important than the absolute values shown in FIGS. **7***a*-**7***b*. To investigate the mole fraction distribution resulting from the flow field, gas chromatographic sampling was carried out along with separate PIV measurement, whose results are shown in FIG. **8**. In this figure, the variations in methane mole fraction along the x coordinate (at y=6.5 mm and z=0 mm) are co-plotted with velocity components, V_x and V_y, at the equivalent locations of the gas sampling for all six geometries. As in FIGS. **7***a*-**7***b*, no flame ignition was attempted for both the sampling and PIV measurements.

[0060] As shown in FIGS. **8***a*-**8***f*, for the R (FIG. **8***a*) and D geometries (FIG. **8***b*), fuel mole fractions are relatively low (~1.8-3.3%) at x<~10 mm where the V_x and V_y velocities are also very low (<~0.1 m/s) while higher velocity (V_y~3 m/s) region coexists with higher fuel mole fraction regions (~5.5%). It is clear that this type of fuel distribution, i.e., high fuel concentration in a high velocity region and vice versa, is not the most efficient way to improve the flame stability. For the local cavity geometries in FIG. **8***d* and FIG. **8***f* (R+S, D+S, and T+S, respectively), on the contrary, the high fuel mole fraction (~5-7%) region is maintained in relatively low-velocity regions (V_y~1-2 m/s, V_x~0-1 m/s), where x<~10 mm, while the mole fraction decreases in the high-velocity region (x>~15 mm). For example, the region of peak mole fraction in the R+S geometry (x~4 mm) shows the velocity, V_y~2 m/s (69% of peak V_y) and V_x~0.8 m/s, while that in the R geometry (x~16 mm) shows velocity, V_y~3 m/s (99% of peak V_y) and V_x~0.1 m/s.

[0061] Another interesting observation is in the gradients of fuel mole fraction. For the R and D geometries, the mole fractions increase by over 100% (from ~2.5% to ~6%) within ~4 mm distance, but for the local cavity geometries, the variations in mole fraction is much smaller, less than 25% in the highest case. It is believed that the way the fuel distributed and the lesser mole fraction gradient in the presence of the local cavities effectively assist in improving blowout limits in the hybrid mode flow.

[0062] Further, regarding FIGS. **8***a*-**8***f*, it is of interest to compare the mole fraction and velocity fields of T (FIG. **8***c*) and T+S (FIG. **8***f*) geometries. The tendencies of the two fields are generally similar for both geometries: the gradual decay of the mole fraction field from ~6 to 4.5% and the gentle increase in V_y up to x~12.5 mm and the asymptotic decrease to the free stream velocity with increasing x. As mentioned earlier, this similarity is caused by the fact that the size of the cavity in the T+S geometry is relatively small. One can still observe some small evidence of the presence of the local cavity from mole fraction data at x~12 mm in the T+S geometry (orange circle). Here, the mole fraction of the T+S geometry is 10% higher than that of T, while the neighboring mole fractions (e.g., at x~10 mm and 14 mm) are almost identical for both geometries. It is believed that this data point further confirms the capability of a local cavity to localize the fuel stream.

[0063] In the following section, the difference in flow fields in the absence/presence of a local cavity will be briefly discussed.

[0064] Turning now to flow fields in the vicinity of the base, FIGS. **9***a*-**9***l* show instantaneous (FIGS. **9***a*-**9***f*) and ensemble averaged (FIGS. **9***g*-**9***l*) PIV images (and pseudo streamlines represented by red lines) of six non-cavity and cavity geometries: R, D and T, and R+S, D+S and T+S. In this particular case, the flame is present and the configuration is the hybrid mode. The flowrate of additional air injection and the resulting nominal flow speed (measured at 2 cm distance away from methane nozzle) are kept identical as 100 SPLM and ~3 m/s, respectively. The equivalence ratio of the fully premixed stream is also kept fixed at 0.72 for all images.

[0065] As shown in the representative instantaneous images (especially R, D, R+S, and D+S), recirculating flow structures, which are believed to play a key role in bluffbody flame stabilization, can be found for all four geometries.

[0066] For example, one can clearly find that the strong recirculating pairs whose centers are at y~10 mm and y~6 mm in the R geometry and y~10 mm and y~20 mm in the D geometry in these specific images. For the R+S and D+S geometries, the structure resides at the height of y~5 mm (R+S) and y~-2 mm (D+S).

[0067] It is interesting, however, that the recirculating pattern is more clearly shown and the strength of the recirculating flow in this region of interest is more intense in the non-cavity geometries than in the cavity geometry cases. It is

likely because either intense recirculation zones of the local cavity geometries reside in a region where the laser light cannot illuminate, e.g., inside of the cavity, and/or the geometries tends to generate small, multiple vortices rather than one large vortex pair (see FIGS. **10***a*-**10***b* for more detailed discussion on the characteristic of vortices generated by each geometry).

[0068] Here, it is noteworthy it was observed that the vortices generated from the local cavity geometries are more incoherent, i.e., the shedding frequency, size, and locations are more variable, as described in our previous study. Evidence of the incoherent vortices can also be found in the present study as shown in the averaged PIV images of FIGS. **9***g*-**9***l*. From the figure, one can observe that the recirculation pattern of non-cavity geometries is still clearly seen (especially R and D), but no apparent vortex is observed in the cavity geometries (R+S and D+S). This fact implies that the vortices observed in instantaneous images of the cavity geometries are more random (incoherent) such that it tends to disappear in the ensemble averaged images.

[0069] Unlike the above four geometries, the T and T+S geometries have more direct (i.e., non-recirculating) flow pattern along the slanted side surfaces in the region of interest for which laser illumination was present. It seems that the flow pattern is inconsistent with our previous observations, which showed two large, nearly symmetric recirculations along the side surfaces in ~5.7 m/s vitiated flow in the absence of additional air injection. It is believed that a slight misalignment between the direction of the fully premixed flow and the air injection in the current configuration induces a small skew of the local flow (to the right) in the region of interest. The skewed flow, as clearly seen in the averaged field, seems to eliminate the recirculation zone on the left face in the region of interest and create bent flow along their vertices at y~0 (clockwise direction). Although it is not shown here, one can see elements of a recirculation zone in the other side (right face) of the T and T+S bases (e.g., near x=y=−5) from the relatively upright averaged flow field at x~-5 to −10, y=0 in FIGS. **9***g*-**9***l*, and the corresponding instantaneous images in FIGS. **9***a*-**9***f*. It is believed that this small asymmetry may be amplified in the geometries such as T and T+S (which show a higher sensitivity to the flow symmetry because of their sharp vertices) and thus alter the flow pattern of those geometries, namely two recirculation bubbles or just a single recirculation bubble.

[0070] According to the current invention, the improvement of the blowout limit in the cavity geometries is due to its ability to distribute the fuel in a less diluted manner, where geometries according to R and R+S and the D, D+S, T and T+S are more robust to the flow asymmetry.

[0071] Turning to FIGS. **10***a*-**10***b*, FIG. **10***a* shows representative instantaneous images of the swirling strength field (the imaginary portion of the complex-conjugate eigenvalues of the local velocity gradient tensor) and pseudo streamlines (represented by white lines) in each of the six geometries (R, D, T, R+S, D+S, and T+S), at experimental conditions that are identical to that of FIGS. **9***a*-**9***l*. It is believed that the swirling strength, a measure of how fast the fluid is rotating locally, is a good marker of vortical structures. As shown in the images, one can find that the number of vortices in the bluffbody downstream of the cavity geometry (and T geometry) is larger than those in the non-cavity geometries (especially comparing the R and R+S, and D and D+S).

[0072] The current invention provides complex back-steps in the geometry to generate multiple and incoherent vortices. In FIG. **10***b*, the swirling strength of the averaged velocity field (shown in FIGS. **9***g*-**9***l*) is illustrated. Note, unlike the instantaneous field in FIGS. **10***a*-**10***f*, no noticeable discrepancy exists between the non-cavity and cavity geometries, i.e., there exists a similar number of diffuse vortices in all six cases. Here, multiple, highly concentrated vortices in an instantaneous field, and a smaller number of diffuse vortices in an averaged field shown in the cavity geometries are formed by local cavity geometries are generated by the incoherent vortices unlike the non-cavity geometries (especially R and D).

[0073] The strain rates of the averaged velocity field in the six example test geometry cases are illustrated in FIGS. **11***a*-**11***f* whose experimental conditions are identical to those of FIGS. **10***a*-**101**. The result presented here shows strong consistency for all cases tested (more than 10 sets of PIV experiments for each geometry), confirming that it is statistically stationary. As shown in the figure, the region of high strain rates is generally large in the non-cavity geometry cases (e.g., see the strain rate on the top surface of R and D geometries) while that in the cavity geometry is minimal (D+S) or small (R+S). The inventors do not believe that this level of strain rate (<~100/s) can cause local extinction, but expect that the high strain rate in the vicinity of the bluffbody seen in the non-cavity geometries is not beneficial in improving the flame stability. Similar to previous observations, no noticeable difference is found between T and T+S geometries.

[0074] FIGS. **12***a*-**12***h*, show embodiments of the current invention that includes a jet engine flame holder bluffbody **1200** having a rounded leading edge **1202**, a mid-body **1204** having a rectangular cross-section, and a trailing edge **1206**, where the trailing edge includes a rectangular cross-section having digitated cutouts **1208** from the rectangular cross-section, where the tailing edge **1206** projects upward according to a digitated cross-section, where material digits **1210** remain between consecutive pairs of the digitated cutouts **1208**. As shown, the trailing edge **1206** has a block-shape along a length of the trailing edge **1206**, with a rectangular recess **1212** along an upper-center portion of the solid body, where each digit is a crenellation feature **1214**. Referring to FIGS. **12***d*-**12***h*, FIG. **12***d* shows a thin-walled trailing edge **1206** crenellation features **1214** having a thickness up to a thickness of the wall of the hollow mid-body **1214**, and a relatively deep rectangular recess **1212**. FIG. **21***e* shows the trailing edge **1206** with tapered crenellation features **1214**, where it is understood that the crenellation shapes shown in FIG. **12***d*, FIGS. **13***a*-**13***h* and FIGS. **14***a*-**14***l* can include tapered sidewalls or edges. FIGS. **12***f*-**12***h* show the crenellation features **1214** having a top surface that is angled towards the rectangular recess **1212** (FIG. **12***f*), angled away from the rectangular recess **1212** (FIG. **12***g*), and a rounded top surface (FIG. **12***h*), respectively.

[0075] In another aspect of the invention, the leading edge **1202**, the mid-body **1204**, and the trailing edge **1206** are hollow structures.

[0076] FIGS. **13***a*-**13***h* show different embodiments of the trailing edge **1206**. According to one aspect of the invention, the trailing edge **1206** is a wedge-shape along a length of the trailing edge, where each digitated cutout **1208** includes a cross-section shape that is square, rectangular, semi-circular, partly-circular, elliptical, or triangular. Further shown, the material digits **1210** can have a cross-section shape that can

be square, rectangular, circular, semi-circular, partly-circular, elliptical, or triangular. In a further aspect of the invention, the material digit **1210** is a triangular shape, where a side of the triangular shape is curved.

[0077] FIGS. **14***a*-**14***k* show features that represent exemplary cutout **1208** cross-sections, material digit **1210** cross-sections or crenellation feature **1214** cross-sections, where the cross-sections **1400** include square, rectangular, semi-circular, partly-circular, elliptical, trapezoidal, parallelogram, pentagonal, hexagonal, plus-sign, curved plus-sign or triangular cross-sections.

[0078] The present invention has now been described in accordance with several exemplary embodiments, which are intended to be illustrative in all aspects, rather than restrictive. Thus, the present invention is capable of many variations in detailed implementation, which may be derived from the description contained herein by a person of ordinary skill in the art. All such variations are considered to be within the scope and spirit of the present invention as defined by the following claims and their legal equivalents.

What is claimed:

1. A jet engine flame holder bluffbody, comprising:

a. a leading edge, wherein said leading edge is rounded;

b. a mid-body, wherein said mid-body comprises a rectangular cross-section; and

c. a trailing edge, wherein said trailing edge comprises said rectangular cross-section having digitated cutouts from said rectangular cross-section, wherein said tailing edge projects upward according to a digitated cross-section, wherein material digits remain between consecutive pairs of said digitated cutouts.

2. The jet engine flame holder bluffbody of claim **1**, wherein said trailing edge comprises a wedge-shape along a length of said trailing edge.

3. The jet engine flame holder bluffbody of claim **1**, wherein said trailing edge comprises a block-shape along a length of said trailing edge.

4. The jet engine flame holder bluffbody of claim **3**, wherein said trailing edge comprises a rectangular recess along an upper-center portion of said solid body, wherein each said digit comprises a crenellation feature.

5. The jet engine flame holder bluffbody of claim **4**, wherein said crenellation feature comprises a cross-section shape selected from the group consisting of square, rectangular, semi-circular, partly-circular, elliptical, triangular.

6. The jet engine flame holder bluffbody of claim **4**, wherein said crenellation feature comprises a top surface selected from the group consisting of angled towards a centerline along a length of said trailing edge, angled away from a centerline along a length of said trailing edge, and rounded.

7. The jet engine flame holder bluffbody of claim **4**, wherein said crenellation feature comprises a tapered sidewall.

8. The jet engine flame holder bluffbody of claim **1**, wherein each digitated cutout comprises a cross-section shape selected from the group consisting of square, rectangular, semi-circular, partly-circular, elliptical, and triangular.

9. The jet engine flame holder bluffbody of claim **1**, wherein said material digits comprise a cross-section shape selected from the group consisting of square, rectangular, circular, semi-circular, partly-circular, elliptical, and triangular.

10. The jet engine flame holder bluffbody of claim **1**, wherein said leading edge comprises a hollow structure.

11. The jet engine flame holder bluffbody of claim **1**, wherein said mid-body comprises a hollow structure.

12. The jet engine flame holder bluffbody of claim **1**, wherein said trailing edge comprises a hollow structure.

13. The jet engine flame holder bluffbody of claim **1**, wherein said material digit comprises a triangular shape, wherein a side of said triangular shape is curved.

14. The jet engine flame holder bluffbody of claim **1**, wherein said trailing edge comprises crenellation structures and a rectangular recess having a wall thickness up to a thickness of a wall thickness of a hollow said mid-body.

* * * * *